Removal of Poly(methyl methacrylate) in Diblock Copolymers Films Studied by Grazing Incidence Small-Angle X-Ray Scattering

Guillaume Freychet,[1,2] Mireille Maret,[3,4] Raluca Tiron,[1,2] Xavier Chevalier,[5] Ahmed Gharbi,[1,2] Marta Fernandez-Regulez,[1,2] Patrice Gergaud[1,2]

[1]University of Grenoble Alpes, Grenoble, F-38000, France
[2]CEA, LETI, MINATEC Campus, Grenoble, F-38054, France
[3]SIMAP, University of Grenoble Alpes, Grenoble, F38000, France
[4]SIMAP, CNRS, Grenoble, F-38000, France
[5]ARKEMA France, Route Nationale 117, Lacq, BP34-64170, France
Correspondence to: M. Maret (E-mail: Mireille.maret@simap.grenoble-inp.fr)

Received 9 December 2015; accepted 25 January 2016; published online 22 February 2016
DOI: 10.1002/polb.24017

ABSTRACT: Self-assembly of diblock copolymers (BCP) into periodic arrays is a promising route to generate templates for the fabrication of nanoscopic elements, when one block is selectively removed. In cylindrical morphology polystyrene-block-poly(methyl methacrylate) (PS-*b*-PMMA) copolymer (BCP) films, the efficiency of different processes for removing the PMMA from cylinders is studied using grazing incidence small angle X-ray scattering (GISAXS), x-ray reflectivity and critical dimension scanning electron microscopy. The detailed analysis of the GISAXS patterns leads to the determination of the depth of cylindrical holes left by removal of the PMMA. It is found that the combination of a preliminary UV exposure followed by a wet treatment allows to remove totally the PMMA blocks. Furthermore, the optimization of both UV exposition time and solvent allows to preserve the PS matrix and interestingly for nanolithographic applications to decrease the process costs. © 2016 Wiley Periodicals, Inc. J. Polym. Sci., Part B: Polym. Phys. **2016**, *54*, 1137–1144

KEYWORDS: copolymers; GISAXS; scanning electron microscopy; self-assembly; thin films; x-ray reflectivity

INTRODUCTION Density multiplication of patterned templates by directed self-assembly (DSA) of block copolymers (BCP) with a possible resolution down to 10 nm stands out as a promising alternative to overcome the limitation of conventional lithography. Thanks to the ease of processing, low manufacturing costs, low critical dimension and high density of achievable features, the study of BCP films is becoming targeted.[1–3]

The structures of diblock copolymer are composed of two chemically distinct blocks which self-organize into periodic arrays of nanostructures whose size and spacing are ranging from 10 to 50 nm. By tuning the composition and molecular weight of BCP, the dimensions and shape of nanostructures including spheres, cylinders, and lamellae can be controlled. After selective removal of one block, the remaining pattern can then be transferred into functional materials.

For the use of self-assembled BCP films in large-scale industrial lithography processes, at least two difficulties have to be overcome. The first one is to control the lateral order of self-assembled microdomains using either surface chemical patterns[4,5] or topographic substrate patterns[6–8] in order to form single-grain domains over large areas. The second one is the total removal of one block while controlling the shape and dimensions of empty features, using different processes (wet treatment, plasma etching or UV exposure).

To characterize precisely the morphology of self-assembled BCP films, Grazing Incidence Small-Angle X-ray Scattering (GISAXS) is indisputably becoming, during the last ten years, a well suited technique bringing statistical information about the size, shape and spatial arrangement of different blocks.[9–16] Recently we have successfully used this technique to examine the guidance effect of a line grating on the self-assembly of polystyrene-block-poly(methyl methacrylate) (PS-*b*-PMMA) copolymer (BCP) films, exhibiting two dimensional (2D) hexagonal symmetry with perpendicularly oriented PMMA cylinders.[17] Here, we take advantage of GISAXS to evaluate the efficiencies of different PMMA removal procedures applied to BCP thin films prepared on Si full sheets. In the scattered intensities, the structure factor describing the 2D hexagonal array prevails on the form factor of cylinders. However along the crystal truncation rods of the 2D

hexagonal array, a signature of the efficiency of the PMMA removal treatment can be revealed.

EXPERIMENTAL

Material

The polystyrene-block-poly(methyl-methacry-late)(PS-*b*-PMMA) diblock copolymer used in this study has a number-average molecular weight equal to 46 kg/mol for PS and 21 kg/mol for PMMA with a dispersity index of 1.11. PS-*b*-PMMA was dissolved in propylene glycol monomethyl ether acetate and spin-coated on the top of a 8.8 nm thick PS-r-PMMA brush layer preliminarily deposited on Si wafers. The styrene volume fraction in PS-*b*-PMMA films and in PS-r-PMMA layer is of about 70%. Both copolymers were supplied by Arkema A rapid thermal annealing up to 240 °C, followed by 10 min dwelling before cooling, leads to the phase separation into a hexagonal array of perpendicular cylinders of PMMA with a lattice period, L_0, around 36 nm. The PS-*b*-PMMA film thicknesses are close to 48 nm.

Characterization Techniques

The surface morphology of BCP films was initially characterized by Critical-Dimension Scanning Electron Microscopy (CD-SEM). The CD-SEM images were recorded using a Hitachi S-9300 CD-SEM. Image acquisition conditions were 800V, 6pA and integration over 128 frames. The total film thicknesses were determined by X-ray reflectivity (XRR) using a Xpert Panalytical equipment with a Cu Kα X-ray source. The Grazing small-angle X-ray scattering (GISAXS) experiments were carried out on the CRG-BM02 beamline at the European Synchrotron Radiation Facilities (ESRF) in Grenoble using a photon energy of 11 keV. The beam size at the sample position is 150 μm high and 300 μm wide. A 2 mm wide Ta strip was used in front of the detector in order to stop the intense incident and reflected (specular) beams. The samples were positioned on a 6 circle-goniometer, for an accurate control of the incident angle versus the film surface. The GISAXS measurements were performed at an incident angle $\alpha_i \approx 0.14^\circ$, that is, slightly larger than the critical angle of the polymer film (0.12°) and lower than the Si one (0.163°). The scattered intensities were recorded with an XPAD pixel detector (960*560 pixels of 130 μm size)[18] mounted on the SAXS bench at a distance of 2990 mm from the sample. To minimize air scattering the whole path of the scattered beam was under vacuum apart from the nearest region around samples. The sample size was 20 $\times$ 20 mm^2. Since the aim of these measurements is to probe the removed quantity of PMMA after specific treatments, short counting times up to 100 s were chosen preventing PMMA degradation under synchrotron radiation, occurring after longer exposure times.[17] As depicted in Figure 1, the incident beam propagating along the x direction, the GISAXS images were recorded in the (q_y, q_z) plane where q_y and q_z are the components of the wave vector transfer q related to the in-plane angle $2\theta_f$ and out-of-plane angle α_f.[19] All patterns were normalized with respect to the incident beam intensity monitored by a front photomultiplier.

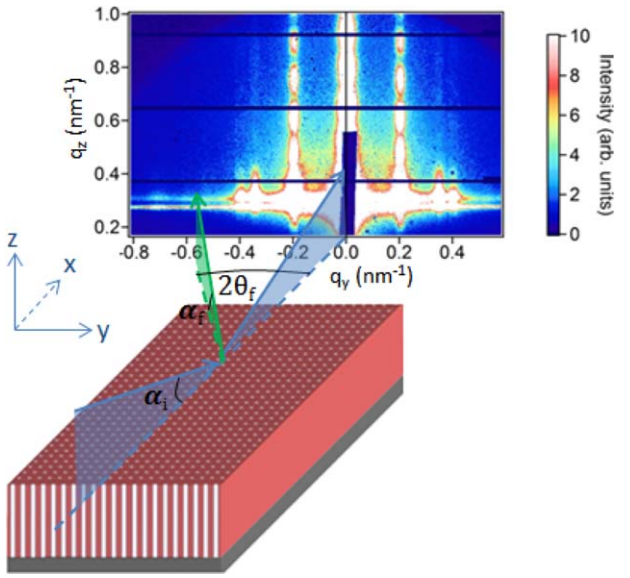

FIGURE 1 GISAXS configuration for a self-assembled PS-*b*-PMMA copolymer film probed under an incident angle α_i. The scattered beam is defined by the in-plane $2\theta_f$, and out-of-plane α_f angles. [Color figure can be viewed in the online issue, which is available at wileyonlinelibrary.com.]

PMMA Removal Strategies

Different methods were previously used to remove selectively PMMA in PS-*b*-PMMA films like acid surface reconstruction, plasma etching or a combination of both methods.[17]

While an acid treatment followed by plasma etching was proven to remove totally PMMA, this evolution is accompanied by an undesirable decrease of the film thickness, due to a simultaneous removal of PS under plasma but with an etching rate three times smaller than for PMMA. Therefore, another way was proposed relying on a preliminary exposure of BCP films to UV radiation, before applying a wet treatment.[20] Such process was previously studied by other research groups[21–24] and the effectiveness of PMMA removal was mainly probed from scanning electron and atomic force microscopies. The advantage of UV exposure is to cut selectively the PMMA chains improving their removal during a further chemical treatment. To validate this new strategy, the duration of UV exposure has to be optimized to avoid cross-links between PS and PMMA which would prevent further selective removal. Moreover, the efficiency of different solvents in the final PMMA removal has to be tested. As an example, the CD-SEM images show the effect of such a double treatment using dimethyl sulfoxide (DMSO), with the formation of characteristic circular holes following the release of PMMA without change of the 2D hexagonal array (Fig. 2).

However, the SEM images provide only surface information and do not account for the efficiency of such combined method in the film volume. Hence, GISAXS measurements are able to bring volume information about the cylindrical hole shape. To determine the best conditions to remove totally the PMMA using such removal process, GISAXS measurements were performed on differently treated samples: (i)

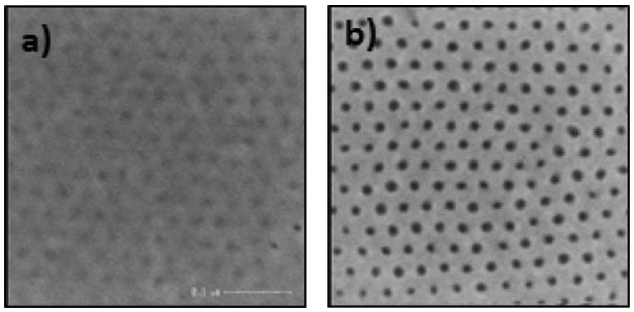

FIGURE 2 Top-view SEM images of self-assembled diblock (PS-*b*-PMMA) copolymer films: (a) no treatment and (b) after 2s UV exposure followed by DMSO etching.

only chemically treated using different solvents, (ii) only UV exposed for different times and (iii) treated in two steps (i.e., UV exposure followed by chemical etching).

GISAXS MEASUREMENTS

Chemical Treatment

The choice of solvent relies on the selectivity between the ether linkage of PMMA and the aromatic hydrocarbon of PS, as already reported by Asakawa *et al.*[25] Our choice was focused from the amphiphilic feature of PS-PMMA copolymers with PS hydrophobic and PMMA hydrophilic domains. First of all, hydrophobic solvents such as the dimethylformamide (DMF) were tested.

The GISAXS patterns (not shown) obtained for films treated with DMF reveal total removal of BCP film. In fact, since hydrophobic solvents are non-polar reactants, they react with PS, pulling out the BCP film from the brush layer. Thus, hydrophobic solvents are not at all suitable for removing selectively PMMA. Consequently, various hydrophilic solvents were preferentially used, such as isopropyl alcohol (IPA), acetic acid and dimethyl sulfoxide (DMSO). The wet treatment took five minutes which was optimized for acetic acid and fulfilled microelectronics requirements The GISAXS patterns of films treated with these 3 solvents are shown in Figure 3(b–d) and can be compared to the one for the untreated film [Fig. 3(a)]. As PMMA is still present, the weak electronic density contrast between PS and PMMA allows only the measurement of the two 10 Bragg rods of the 2D hexagonal array formed by the PMMA cylinders, observed for the untreated sample but also for the IPA treated sample. From the 10 rod position, the period of the hexagonal array, L_0, deduced following the general relation: $\frac{1}{d_{hk}^2} = \frac{4}{3}\frac{h^2+hk+k^2}{L_0^2}$, is equal to 36.20 nm. This value is somewhat larger than the

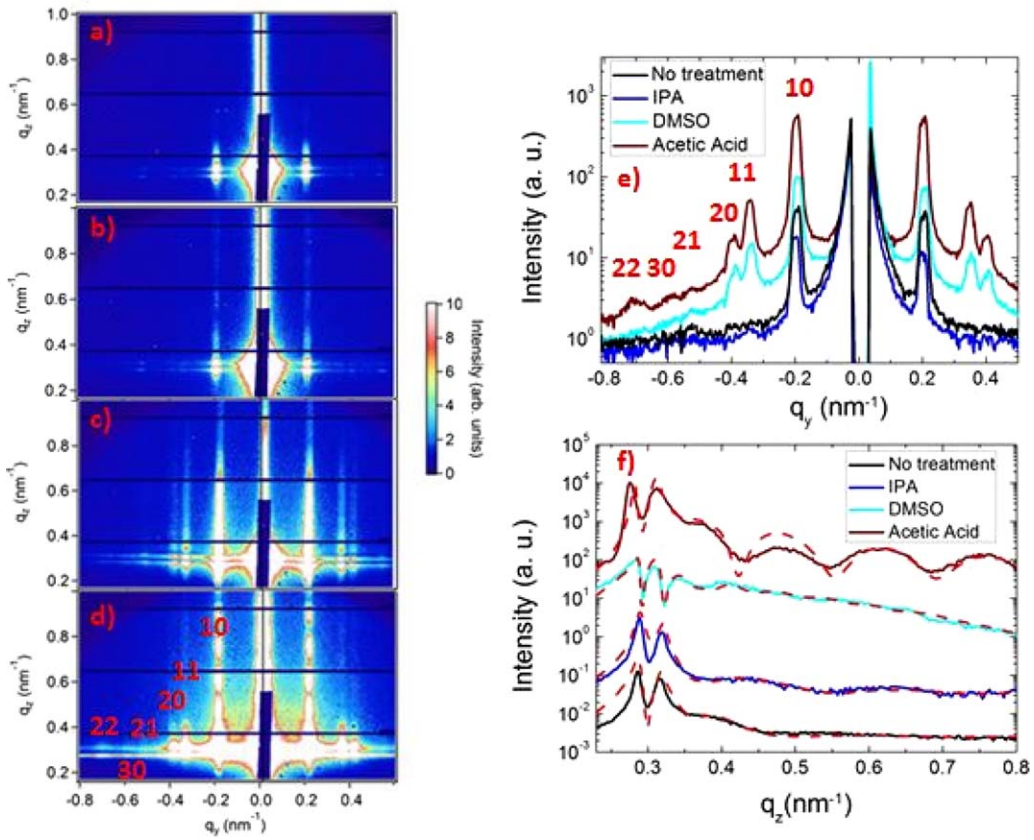

FIGURE 3 GISAXS patterns of self-assembled (PS-*b*-PMMA) BCP films (a) before and after 5min long treatment with (b) IPA, (c) Acetic Acid and (d) DMSO. (e) Intensity profiles along q_y around the Yoneda peak of Si ($q_z = 0.31$ nm^{-1}). (f) Intensity profiles along the 10 Bragg rod: experimental curves (solid) and simulated ones (dashed). [Color figure can be viewed in the online issue, which is available at wileyonlinelibrary.com.]

TABLE 1 Main structural parameters of the BCP films extracted from GISAXS, CD-SEM and XRR measurements as a function of the etching treatment: L_0 and D are, respectively, the polymer period and cylinder diameter, t the thickness of the BCP film (after subtracting the brush layer thickness from the total thickness deduced from XRR) and σ its roughness, and H the cylindrical hole height (*superficial holes cannot be totally excluded)

	CD-SEM		Reflectivity		GISAXS		
Etching treatment	L_0, nm	D, nm	t, nm	σ, nm	L_0, nm	D, nm	H, nm
No treatment	34.9	12.8	47.9	0.9	36.3	11–13	0
IPA	34.6	14.2	47.6	0.8	36.2	11–13	0*
Acetic Acid	34.6	12.0	51.2	1.2	36.2	11–13	44
DMSO	34.7	10.3	Not measured		36.2	11–13	9.0

one deduced from CD-SEM images (Table 1). This difference can be explained by a change of the PS matrix under the high energy electron beam inducing a cross linking of the PS matrix but also to the calibration of the CD-SEM measurements.

After DMSO and acetic acid treatments, the increase of the 10 rod intensity and the appearance of higher order rods at positions characteristic of the 2D hexagonal array indicates that a large amount of PMMA was removed from cylinders leading to an enhanced electronic contrast between the resulting cylindrical holes and PS matrix. Moreover, the measurement of all hk rods, as labeled in Figure 3(d), is the signature of randomly oriented domains with hexagonal symmetry. Figure 3(e) shows the intensity profiles along q_y calculated at $q_z = 0.31$ nm^{-1}, (i.e., at the Si Yoneda peak) for all films. It turns out that in spite of PMMA removal the positions of the 10 Bragg rods stay unchanged at +(-)0.2 nm^{-1}. In contrast with previous GISAXS experiments for similar BCP films,[17] no rod extinction is observed for the DMSO and acetic acid treated samples. Such effect occurs when one rod position matches with a minimum in the form factor whose position is characteristic of a specific cylinder diameter. However, the analysis of SEM images lead to average diameters equal to 10.3 and 12 nm for DMSO and acetic acid, consistent with the presence of the 20 and 12 rods whose extinction would correspond to cylindrical holes with diameters of 13 and 11 nm, respectively. Figure 3(f) shows the intensity profiles along q_z calculated along the 10 rod. For the untreated film a good representation of its profile using the FitGISAXS software[26] was obtained assuming PMMA-filled cylinders with an average height of 46nm. The first bump after the two Yoneda peaks comes mostly from the form factor of cylinders, but due to the weak contrast between PS and PMMA, its oscillations at higher q_z cannot be detected. The linecut of the IPA treated sample is similar to that obtained for the untreated sample and a good fit was obtained with a cylinder height of 42 nm. In contrast, the profile intensities for the films treated with DMSO and acetic acid are much higher, consistent with the enhanced contrast between cylindrical holes and the PS matrix [Fig. 3(f)]. Nevertheless the shape of these two intensity profiles differs considerably. The pronounced oscillations for the acetic acid treated sample are well represented by cylindrical holes with a depth of 44 nm. After DMSO treatment the intensity profile is characterized above the Yoneda peaks by weak oscillations of short period superimposed on a slowly decreasing signal. The slow damping in intensity can be attributed to the form factor of shallow holes and the oscillations to the waveguiding interference of the scattered photons between the two interfaces (air/BCP and BCP/Si) as already reported for different layered systems.[27,28] The values of the hole heights (Table 1) are listed together with the thicknesses (t) and surface roughnesses (σ) of BCP films, obtained from the best fits of the reflectivity measurements (Fig. 4) using Xpert software. Due to the negligible electronic contrast between the brush layer and the self-assembled film, only one total thickness can be extracted from simulations. Thus, the values in Table 1 refer to the thicknesses of the self-assembled films after subtracting the 8.8 nm thickness of the brush layer from the total thickness.

The largest surface roughness is found for the acetic acid treated sample leading to the marked damping of the Kiessig fringes. It can be attributed to remaining PMMA chains around the cylindrical holes.[20,29] In fact, the amphiphilic feature of the BCP film and the hydropholic property of solvent

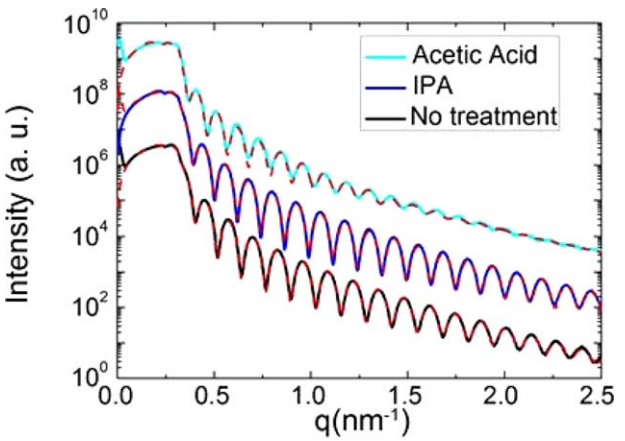

FIGURE 4 Experimental (solid lines) and simulated (red dashed lines) reflectivity curves of the same BCP films as those measured by GISAXS: not treated film (black line), after IPA (blue line) and acetic acid (cyan line) treatments (the curves are shifted for clarity). [Color figure can be viewed in the online issue, which is available at wileyonlinelibrary.com.]

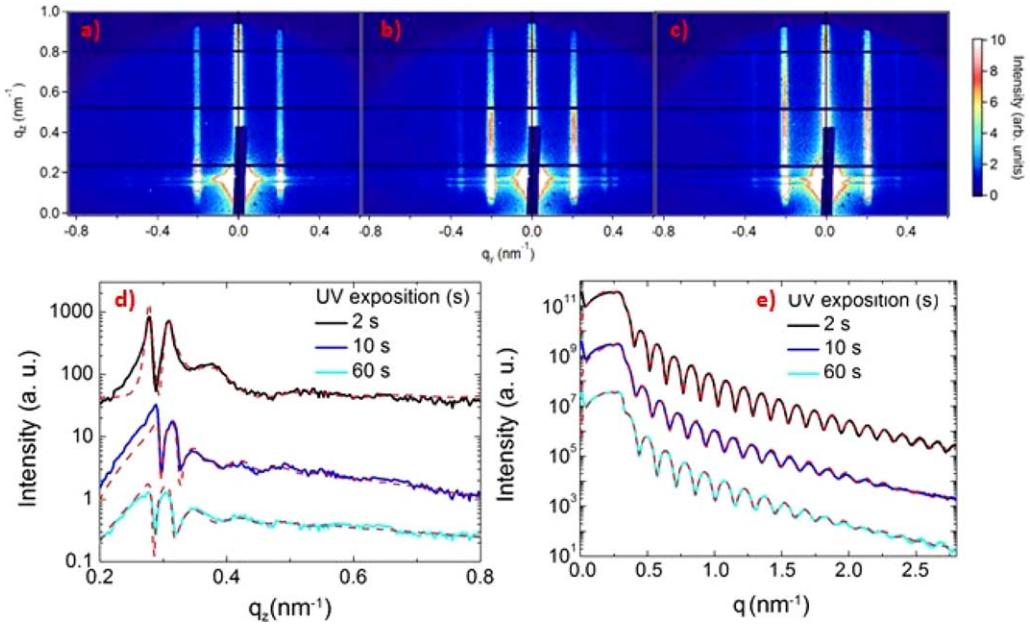

FIGURE 5 GISAXS patterns of diblock (PS-*b*-PMMA) copolymers after UV exposure for 2 s (a), 10 s, (b) and 60 s (c). (d) Intensity profiles along the 10 rod: experiment (solid) and simulations (red dashed) using FitGISAXS software. (e) Experimental (solid) and simulated (red dashed) reflectivity curves. For clarity the curves in (d) and (e) are shifted. [Color figure can be viewed in the online issue, which is available at wileyonlinelibrary.com.]

lead to a strong affinity with PMMA and a repulsion with PS. The combination of both effects promotes PMMA migration from cylinders to the surface but remaining attached to PS at the surface and on the cylindrical side-walls. The comparison between the hole heights and BCP film thicknesses reveals that among the three solvents, acetic acid, due to its nonpolar acid complex, is by far the most efficient to remove the PMMA, but not perfectly as discussed above. With IPA and DMSO longer treatment times would have led to better removal performances.

A pure chemical treatment is thus insufficient to remove totally PMMA. To overcome such limitation, the idea is to submit previously the BCP films to UV exposure whose radiation energy would lead to the degradation of the PMMA-blocks via chain scission.

UV Exposure

In order to evaluate precisely the UV impact on the morphology of the BCP films, different exposure times were tested (0, 2, 5, 10, 30, 60 s). Figure 5(a–c) shows the most representative GISAXS patterns obtained for films exposed to UV for 2, 10 and 60 s. In comparison with the pattern of the untreated film [Fig. 3(a)], a marked increase of the 10 rod intensity and after 10s the appearance of higher order rods are observed, suggesting partial PMMA removal. However, the analysis of the vertical linecuts calculated along the 10 rod indicates that PMMA removal stops roughly after 30 s exposure time.

As previously observed, characteristic differences in the oscillations of linecuts deserve to be underlined [Fig. 5(d)]. After the two Yoneda peaks, for the 2 s UV sample a marked bump is measured, while the profiles obtained beyond 5 s exposure present oscillations of smaller amplitude with an overall slow decrease with q_z. Good simulations of 2s linecut were obtained assuming cylinders full of PMMA as it was done for the IPA treated sample [see Fig. 3(f)]. In contrast, the linecuts for the 10 and 60s exposed samples are well represented assuming shallow holes stemming from partial PMMA removal which give rise to the slow decrease with q_z. The weak oscillations are attributed to waveguiding interference effects which are well represented using the film thicknesses deduced from the reflectivity measurements [Fig. 5(e)]. Estimates of the hole depths are given in Table 2, together with the thicknesses and surface roughnesses of BCP films. It turns out that UV exposure starts to have a significant effect on PMMA removal from 5 s exposure. Compared to the film thicknesses, such effect remains localized

TABLE 2 Variation of the BCP film thickness (after subtracting the brush thickness), *t*, roughness, σ, and cylindrical hole height, *H*, with UV exposure time

UV exposition time (s)	Reflectivity		GISAXS
	t, nm	σ, nm	*H*, nm
0	47.9	0.9	0
2	46	1	0
5	45.4	1	6
10	44.3	1.2	6
30	41.6	1.1	6
60	40.8	1.1	5.5

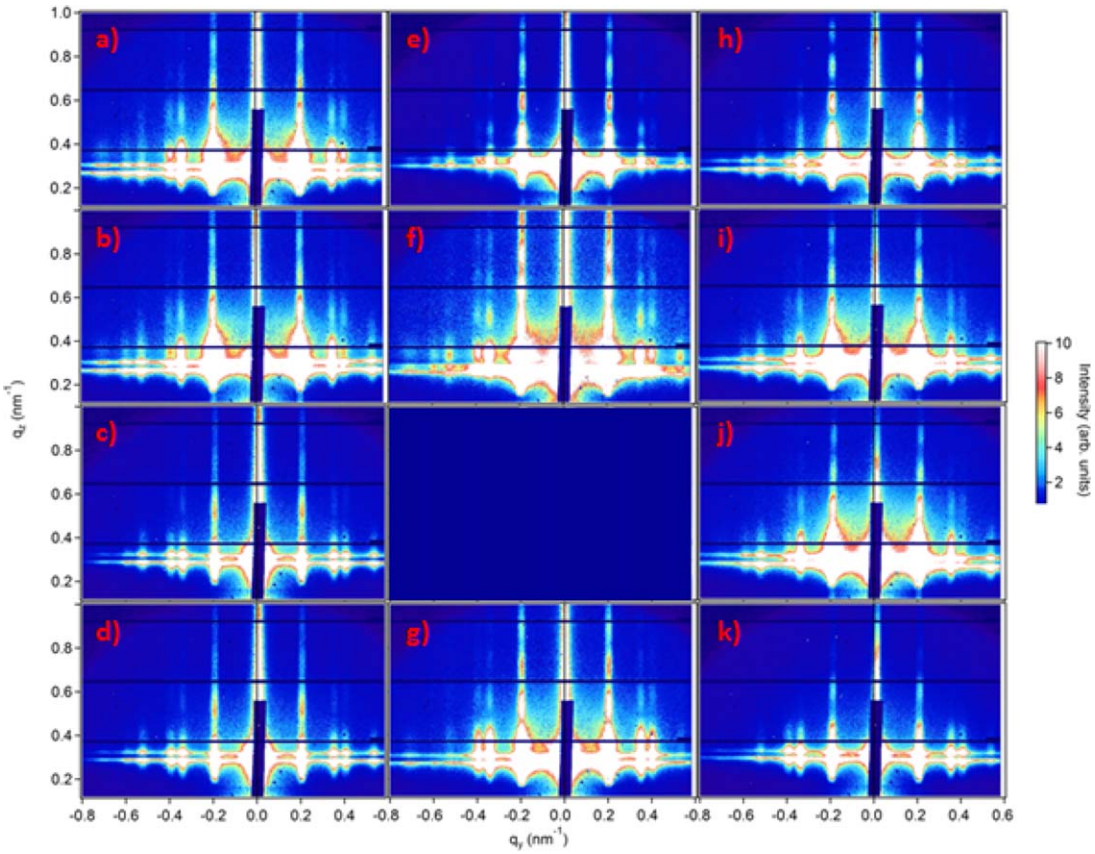

FIGURE 6 GISAXS patterns of BCP films, UV exposed for 2 s, 5 s, 10 s, and 30 s (from the first to the last row), and chemically treated using: (a–d) IPA, (e–g) acetic acid, and (h–k) DMSO. [Color figure can be viewed in the online issue, which is available at wileyonlinelibrary.com.]

at the film surface, since no drastic change of the hole depth with exposure time is observed. Even after 60 s the depth tends to decrease. The UV radiation energy supplied to the BCP films permits to break the links between PS and PMMA chains and to remove PMMA especially at the film surface.

However, after long exposure times, cumulative UV radiation energy produces cross-linking between the two blocks leading to an increase of film density. Such behavior is consistent with a regular decrease of the film thickness with exposure time, as deduced from the reflectivity measurements (Table 2). These cross-linking effects slow down considerably the PMMA removal until to prevent it totally after long exposures. It is worth noting that even after 2 s exposure a significant decrease of the film thickness is nevertheless observed. From these measurements, it appears that only UV exposure cannot achieve a complete PMMA removal. Taking advantage of such effect, a coupled UV exposure-chemical treatment process would be an attractive route. The conjugated effects of exposure time and nature of solvent are examined in the next section.

Combination of UV and Chemical Treatments

To reach the most effective conjugated process, BCP films treated with IPA, DMSO and acetic acid after various UV exposure times were measured by GISAXS and XRR. An overview of the variation of the PMMA removal efficiency is illustrated by the series of GISAXS patterns shown in Figure 6. With all solvents, a preliminary UV exposure for times ranging from 2 s to 10 s favors considerably PMMA removal. In comparison with patterns shown in Figure 3, all Bragg rods are clearly observed, as a consequence of the high electronic contrast between the PS matrix and deep holes created by important PMMA removal. For all solvents, only 2 s exposure already favors the PMMA removal confirming that even short exposures lead to some scission of PMMA chains. The hole heights obtained after the different conjugated processes were extracted from the best simulations of the vertical cuts along the 10 rods, as illustrated in Figure 7 for films treated with IPA. XRR measurements were also performed leading to the final film thicknesses. These values are reported in Table 3 for each differently treated film. Interestingly, the height of removed PMMA after 2 s is superior to that obtained after 30 s exposure, confirming that "cross-linking" between the PS and PMMA chains occurs already after 30 s reducing afterwards the efficiency of a wet treatment

Since for DMSO and IPA the hole heights and the film thicknesses are similar after a 10 s UV exposure, the interest of such two-step process is really demonstrated. However, to

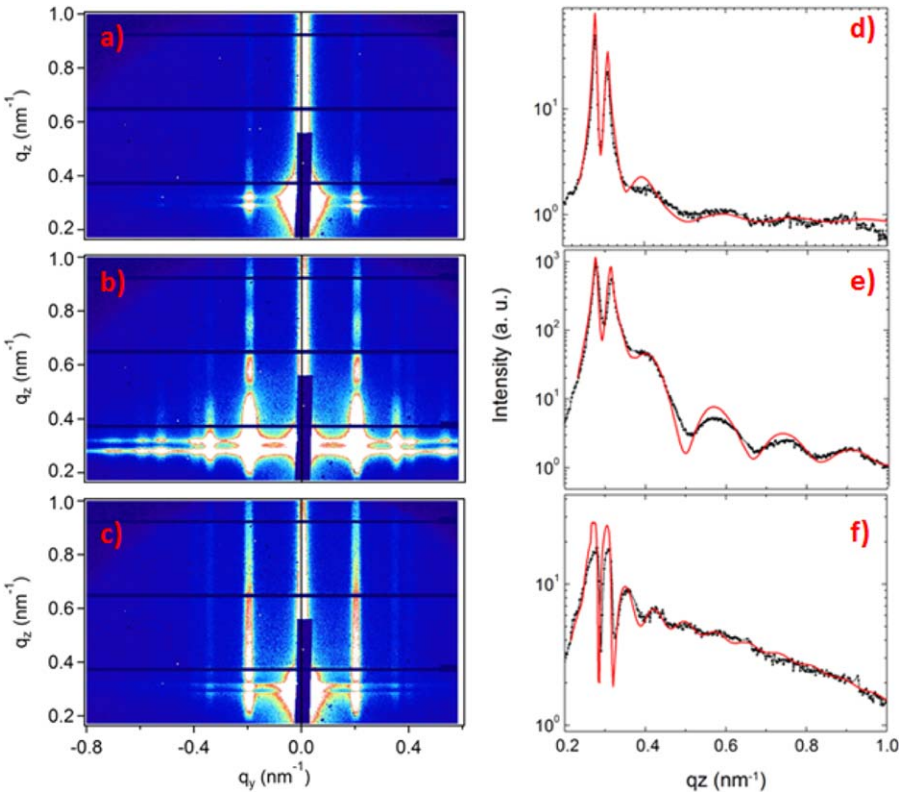

FIGURE 7 GISAXS patterns of BCP films after: (a) 0 s, (b) 10 s, (c) 60 s UV exposure followed by IPA treatment. From (d) to (f) the corresponding intensity profiles along the 10 rod (black lines) and the best fits (red curves) obtained with FitGISAXS software. [Color figure can be viewed in the online issue, which is available at wileyonlinelibrary.com.]

reduce the duration of this process and its cost, DMSO and acetic acid are more favorable than IPA, since they are able to remove all PMMA after a preliminary UV exposure of only 2 s.

In summary, UV pre-treatment is really effective for short exposure times (lower than 30 s). For 60 s exposure, strong cross linking occurs between the two blocks preventing PMMA removal by subsequent chemical treatment. As illustrated in Figure 7(f), the average height of the empty cylinders is only of 3.6 nm after subsequent IPA treatment.

Finally, we have succeeded to remove the whole PMMA after a 2s UV exposition using acetic acid or DMSO. Nevertheless, in order to limit the film degradation and the cost of UV treatment, other polar solvents with a better selectivity between PS and PMMA are still tested.

TABLE 3 BCP film thicknesses (after subtracting the brush thickness), *t*, and cylindrical hole heights, *H*, extracted from XRR and GISAXS measurements

UV	IPA		Acetic Acid		DMSO	
exposure (s)	*t*, nm	*H*, nm	*t*, nm	*H*, nm	*t*, nm	*H*, nm
2	42.4	36.2	38.9	39.0	38.1	38.2
5	40.6	38.0	38.0	38.2	35.7	35.8
10	39.3	38.2	37.6		35.3	35.4
30	35.7	33.6	35.1	34.2	35.3	30.0
60	35.1	3.6	34.8	7.2	34.9	8.4

CONCLUSIONS

The GISAXS measurements on cylindrical morphology PS-*b*-PMMA copolymers, completed by x-ray reflectivity measurements have permitted a well-defined internal structure characterization of the hexagonal array of cylinders, while CD-SEM observations have provided estimates of cylinder diameters at the film surface. Simulations of the 10 Bragg rod intensity profiles of the hexagonal array lead to reliable values of heights of cylindrical holes obtained after different PMMA removal processes. A very short UV exposure followed by a chemical treatment was proven to totally remove the PMMA chains from PS-*b*-PMMA thin films. Such a coupled process is indeed a promising route for the use of self-assembled BCP films as patterns in nanolithography.

ACKNOWLEDGMENTS

Allocation of beamline on the French CRG-BM02 beamline at the ESRF is gratefully acknowledged. The authors thank Silicon Technologies Division (CEA-LETI) for thesis funding. ARKEMA is also acknowledged for providing the PS-*b*-PMMA and PS-r-PMMA copolymers. The authors specially thank D. Babonneau for enlightening discussions about the FitGISAXS software, and

N. Boudet and N. Blanc for their help at BM02. This work was supported by the French National Research Agency (ANR) through the "Recherche Technologie de Base" program.

REFERENCES

1 J. Y. Cheng, C. A. Ross, H. I. Smith, E. L. Thomas, *Adv. Mater.* **2006**, *18*, 2505–2521.

2 H. C. Kim, S. M. Park, W. D. Hinsberg, *Chem. Rev.* **2010**, *110*, 146–177.

3 S. B. Darling, *Prog. Polym. Sci.* **2007**, *32*, 1152–1204.

4 S. Ouk Kim, H. H. Solak, M. P. Stoykovich, N. J. Ferrier, J. J. de Pablo, P. F. Nealey, *Nature* **2003**, *424*, 411–414.

5 M. P. Stoykovich, M. Müller, S. O. Kim, H. H. Solak, E. W. Edwards, J. J. de Pablo, P. F. Nealey, *Science* **2005**, *308*, 1442–1446.

6 R. A. Segalman, A. Hexemer, E. J. Kramer, *Macromolecules* **2003**, *36*, 6831–6839.

7 J. Y. Cheng, A. M. Msayes, C. A. Ross, *Nature Mater.* **2004**, *3*, 823–828.

8 R. Tiron, X. Chevalier, C. Couderc, J. Pradelles, J. Bustos, L. Pain, C. Navarro, S. Magnet, G. Fleury, G. Hadziioannou, *J. Vac. Sci. Technol. B* **2011**, *29*, 06F206

9 D. M. Smilgies, P. Busch, C. M. Papadakis, D. Posselt, *Synchrotron Radiat News* **2002**, *15*, 35–42.

10 P. Müller-Buschbaum, *Anal. Bioanal. Chem.* **2003**, *376*, 3–10.

11 B. Lee, I. Park, J. Yoon, S. Park, J. Kim, K. W. Kim, T. Chang, M. Ree, *Macromolecules* **2005**, *38*, 4311–4323.

12 P. Busch, D. Posselt, D. M. Smilgies, M. Rauscher, C. M. Papadakis, *Macromolecules* **2007**, *40*, 630–640.

13 J. Yoon, S. Y. Yang, B. Lee, W. Joo, K. Heo, J. K. Kim, M. Ree, *J. Appl. Crystallogr.* **2007**, *40*, 305–312.

14 R. Guo, E. Kim, J. Gong, S. Choi, S. Ham, D. Y. Ryu, *Soft Matter* **2011**, *7*, 6920–6925.

15 V. Mishra, E. J. Kramer, *Macromolecules* **2013**, *46*, 977–987.

16 A. Hexemer, P. Muller-Buschbaum, *IUCrJ.* **2015**, *2*, 106–125.

17 M. Maret, R. Tiron, X. Chevalier, P. Gergaud, A. Gharbi, C. Lapeyre, J. Pradelles, V. Jousseaume, G. Fleury, G. Hadziioannou, N. Boudet, C. Navarro, *Macromolecules* **2014**, *47*, 7221–7229.

18 J. F. Berar, N. Boudet, P. Breugnon, B. Caillot, B. Chantepie, J. C. Clemens, P. Delpierre, B. Dinkespiller, S. Godiot, C. Meessen, M. Menouni, C. Morel, P. Pangaud, E. Vigeolas, S. Hustache, K. Medjoubi, *Nucl. Instrum. Methods Phys. Res. A* **2009**, *607*, 233–235.

19 M. Maret, F. Liscio, D. Makarov, J. P. Simon, Y. Gauthier, M. Albrecht, *J. Appl. Crystallogr.* **2011**, *44*, 1173–1181.

20 A. Gharbi, R. Tiron, P. Pimenta Barros, M. Argoud, I. Servin, X. Chevalier, C. Nolet, C. Navarro, *J. Vac. Sci. Technol. B* **2015**, *33*, 051602

21 T. Thurn-Albrecht, R. Steiner, J. De Rouchey, C. M. Stafford, E. Huang, M. Bal, M. Tuominen, C. J. Hawker, T. P. Russell, *Adv Mater.* **2000**, *12*, 787

22 K. W. Guarini, C. T. Black, K. R. Milkove, R. L. Sandstrom, *J. Vac. Sci. Technol. B* **2001**, *19*, 2784

23 K. W. Guarini, C. T. Black, S. H. I. Yeung, *Adv Mater.* **2002**, *14*, 1290

24 M. Muramatsu, M. Iwashita, T. Kitano, T. Toshima, M. Somerwell, Y. Seino, D. Kawamura, M. Kanno, K. Kobayashi, T. Azuma, *J. Micro/Nanolithogr. MEMS, MOEMS.* **2012**, *11*, 031305

25 K. Asakawa, T. Hiraoka, *Jpn. J. Appl. Phys.* **2002**, *41*, 6112

26 D. Babonneau, *J. Appl. Crystallogr.* **2010**, *43*, 929–936.

27 D. Babonneau, S. Camelio, D. Lantiat, L. Simonot, A. Michel, *Phys. Rev. B* **2009**, *80*, 155446

28 S. Narayanan, D. R. Lee, R. S. Guico, S. K. Sinha, J. Wang, *Phys. Rev. Lett.* **2005**, *94*, 145504

29 I. Servin, R. Tiron, A. Gharbi, M. Argoud, K. Jullian, G. Chamiot-Maitral, P. P. Barros, X. Chevalier, J. Belledent, X. Bossy, S. Moulis, C. Navarro, G. Cunge, S. Barnola, M. Asai, C. Pieczulewski, *Jpn. J. Appl. Phys.* **2014**, *53*, 06JC05